Research Article

Received: 23 July 2019 Revised: 18 November 2019 Accepted article published: 13 January 2020 Published online in Wiley Online Library:

(wileyonlinelibrary.com) DOI 10.1002/pi.5972

Acetophenone and thiophene side-arm polyaryleneethynylene conjugated polymers for enrichment of electronic applications

Gunasekaran Arun Kumar,[a] Ayyavu Chandramohan,[b] Ponnaiah Gomathi Priya[a] and Muthukaruppan Alagar[c*]

Abstract

In the present work, a new type of semiconducting acetophenone and thiophene side-arm based polyaryleneethynylene (PAE) conjugated polymers (CPs) were synthesized using the Heck–Sonogashira cross-coupling reaction. The new type of monomers and $APAEC_8$, $APAEC_{12}$, $APAEF_8$, $TPAEC_8$, $TPAEC_{12}$, and $TPAEF_8$ (PAE CPs) were synthesized and characterized using Fourier transform IR, NMR and high resolution mass spectrometry studies. The average molecular weight of the CPs was determined using gel permeation chromatography. The data obtained from optical properties in the UV–visible and photoluminescence spectral studies were used to calculate the values of the Stokes shift. Among the six CPs studied, $TPAEC_8$ was found to possess a lower optical band gap ($E_g = 2.112$ eV) than those of the other CPs. The data obtained from different studies, it was found that $TPAEC_8$ exhibits better properties than the other CPs and can be used in the field of organic based photonic, electronic and other sensor applications.

Supporting information may be found in the online version of this article.

Keywords: conjugated polymer; photoluminescence; Stokes shift; electrochemical; optical

INTRODUCTION

Organic conjugated polymer (CP) based materials are quite interesting at present with considerable attraction for their material stability and easy processability with better semiconducting behaviour. The fast growing electronics field requires more and more power for its sustainability. Currently, CPs of polyarylenevinylene and polyaryleneethynylene (PAE) play an important role in energy, memory[1] and display applications.[2] In this context, the electron donating tendency of donor (D) units and the electron withdrawing tendency of acceptor (A) units of PAE CPs are very attractive due to the presence of uninterrupted vacant p-orbital, electron excitation and recombination characteristics. In the D–A units of CPs, the introduction of functional groups in the monomers plays a significant role in the improvement of material properties.[3,4] In this scenario, the poor solubility of rigid PAE CPs is overcome by the introduction of alkyl chains in the CPs. With the improved solubility behaviour of PAE CPs, they are mostly used in printing[5,6] and device fabrication for natural energy conversion.[7] These notable properties of PAE CPs have attracted many researchers to take up active research in the development of D–A PAE CPs using the palladium cross-coupling reaction of the Sonogashira coupling method.[8]

The naturally available chalcones play a beneficial role in anticancer activity,[9–11] bioluminescence[12,13] and active plant resistance[14] of biological applications. However, the synthetic chalcone monomers have attractive features in host–guest chemistry[15] and optical[16] applications. Moreover, the photodimerization behaviour of chalcone based dimethacrylate compounds has been observed by Choi and Oh.[17] An aligned film of chalcone side chain polymer has been investigated by polarized UV irradiation for flat panel applications.[18,19] Benzimidazole-indole-chalcone based side-arm methacrylate polymers have been investigated for organic photovoltaics.[20] Chalcone based materials have been used for the development of four-bit information storage systems.[21] Recently, Song *et al.* have studied amplification of the circularly polarized luminescence of *β*-hydroxyl chalcone based PAE CPs. With existing data, there are only few reports available on the synthesis of a chalcone moiety containing D–A PAE CPs and their optical and electrochemical properties. Hence, in the present study, the simple para-acetyl and para-substituted chalcone based phenylethynylene side-arm D–A two-dimensional PAE CPs were synthesized and characterized by different analytical methods. Photophysical and electrochemical data obtained for the PAE CPs ($APAEC_8$,

* *Correspondence to: M. Alagar, Polymer Engineering Laboratory, PSG Institute of Technology and Applied Research, Neelambur, Coimbatore 641062, India. E-mail: mkalagar@yahoo.com*

a *Department of Chemical Engineering, Alagappa College of Technology, Anna University, Chennai, India*

b *Department of Chemical Engineering, SSN College of Engineering, Chennai, India*

c *Polymer Engineering Laboratory, PSG Institute of Technology and Applied Research, Coimbatore, India*

$APAEC_{12}$, $APAEF_8$, $TPAEC_8$, $TPAEC_{12}$ and $TPAEF_8$) from different studies are discussed and reported.

EXPERIMENTAL

Materials

All precursor chemicals, reagents and solvents were purchased from Merck, Sigma Aldrich, Alfa Aesar, Avra and Fisher Scientific(Tamilnadu, India) and were used for the synthesis. Acetonitrile, *N*,*N*-dimethylformamide, chloroform ($CDCl_3$), dichloromethane and tetrahydrofuran (THF) were purified using phosphorus pentoxide (P_2O_5), calcium hydride (CaH_2) and sodium wire with benzophenone and then distilled under reduced pressure. The zero valent palladium catalyst of tetrakis(triphenylphosphine)palladium(0) ($Pd(PPh_3)_4$), bis(triphenylphosphine) palladium(II) dichloride ($Pd(PPh_3)_2Cl_2$) and copper(I) iodide (Cu(I)I) were purchased from Alfa Aesar. The analytical grades of triethylamine (TEA), methanol and ethanol were distilled under vacuum conditions. Glassware and apparatus were washed and rinsed with acetone followed by a dry nitrogen flush and vacuum. The progress of reactions was monitored through the thin layer chromatographic technique with a suitable eluent. After the work-up, the crude products were purified using a silica gel (100–200 mesh size) column chromatograph.

Sample analysis

The functional group and molecular structure of the synthesized compounds were confirmed using Fourier transform IR (FTIR) spectroscopy and ^1H, ^{13}C and DEPT (distortionless enhancement of polarization transfer) 135 NMR spectrometry. The molecular weight of the monomers were determined using high resolution mass spectrometry, and the average molecular weight of the CPs was determined by gel permeation chromatography (GPC), using polystyrene as an internal standard. The photophysical and electrochemical properties of the PAE CPs were determined with the help of UV–visible spectroscopy, photoluminescence (PL) spectroscopy and cyclic voltammetry measurement. The thermal behaviour of side-arm PAE CPs was studied by TGA at a heating rate of 10 °C min^{-1} from 30 to 800 °C under a continuous flow of nitrogen and the surface morphology of the polymers was analysed by XRD and SEM.

Spectral studies: acceptor and donor monomers

1,4-dibromo-2-iodobenzene

^1H NMR (300 MHz, $CDCl_3$): δ 7.97 (d, 1H, J = 1.5 Hz), 7.44 (d, 1H, J = 8.7 Hz) and 7.31 (d, 1H, J_1 = 8.7 Hz, J_2 = 1.8 Hz).

1-(4-ethynylphenyl) ethanone

^1H NMR (500 MHz, $CDCl_3$): δ 7.92 (d, 2H, J = 8.5 Hz), 7.58 (d, 2H, J = 8.5 Hz), 3.27 (s, 1H) and 2.61 (s, 3H).

1-(4-((2,5-dibromophenyl)ethynyl)phenyl) ethanone

^1H NMR (300 MHz, $CDCl_3$): δ 7.68 (s, 1H), 7.6 (d, 2H, J = 6.6 Hz), 7.47 (d, 1H, J = 8.4 Hz), 7.71 (q, 3H, J = 18 Hz) and 3.80 (s, 2H).

1-(4-((2,5-bis((trimethylsilyl)ethynyl)phenyl)ethynyl)phenyl) ethanone

^1H NMR (300 MHz, $CDCl_3$): δ 7.43 (s, 1H), 7.36 (d, 2H, J = 8.1 Hz), 7.24 (d, 1H, J = 8.1 Hz), 7.17–7.12 (m, 3H), 3.58 (s, 2H), 0.08 (s, 9H) and 0.065 (s, 9H).

1-(4-((2,5-diethynylphenyl)ethynyl)phenyl) ethanone

^1H NMR (300 MHz, $CDCl_3$): δ 7.88 (d, 2H, J = 8.1 Hz), 7.57 (t, 3H, J = 8.7 Hz), 7.42 (d, 1H, J = 8.1 Hz), 7.34 (d, 1H, J = 8.1 Hz), 3.41 (s, 1H), 3.13 (s, 1H) and 2.54 (s, 3H).

1-(4-((2,5-diethynylphenyl)ethynyl)phenyl)-3-(thiophen-2-yl)prop-2-en-1-one

^1H NMR (300 MHz, $CDCl_3$): δ 7.70 (d, 4H, J = 10.2 Hz), 7.64–7.58 (m, 4H), 7.5 (d, 1H, J = 7.8 Hz), 7.41 (d, 1H, J = 7.8 Hz), 7.17 (t, 1H, J = 4.5 Hz), 3.48 (s, 1H) and 3.2 (s, 1H).

1,4-diiodo-2,5-bis(octyloxy) benzene

^1H NMR (500 MHz, $CDCl_3$): δ 7.2(s, 2H), 3.95 (t, 4H, J = 7.5 Hz) and 1.83–0.95 (m, 30H).

1,4-bis(dodecyloxy)-2,5-diiodobenzene

^1H NMR (300 MHz, $CDCl_3$): δ 7.17 (s, 2H), 3.92 (t, 4H, J = 7 Hz), 1.84–1.75 (m, 4H), 1.57–1.27 (m, 36H) and 0.89–0.86 (m, 6H).

2,7-diiodo-9,9-dioctyl-9H-fluorene

^1H NMR (300 MHz, $CDCl_3$): δ 7.45 (d, 4H, J = 8.7 Hz), 7.20 (d, 2H, J = 7.8 Hz), 1.71 (q, 4H, J = 9.45 Hz), 1.068–0.66 (m, 26H) and 0.64 (s, 4H).

POLYMERIZATION

Reacting the aryl halogen with the terminal proton of the alkyne group induces carbon–carbon coupling through the Sonogashira cross-coupling reaction (Schemes 1 and 2) which is an important step in the synthesis of monomers and polymers. In this method, palladium metal catalyst plays a vital role in enhancing the selectivity, reaction rate and the yield of monomers and polymers. In order to achieve high molecular weight polymers, the following procedure was carried out. A dry, ultraclean 25 mL double necked round bottomed flask was used and a Teflon coated magnetic bar was placed with a reflux condenser and dry nitrogen Schlenk line for back filling of nitrogen gas. The set-up was charged with iodo substituted monomer (1 mole equiv) (Appendix S1), terminal free hydrogen ethynylene substituted monomer (1 mole equiv), $Pd(PPh_3)_4$ (0.03 mole equiv) and Cu(I)I (0.06 mole equiv). The TEA (0.5 mL) and dry THF (3 mL) were added to the above reaction mixture in a sequential order. Initially, the reaction mixture was heated to 50 °C for activation, and then the whole reaction was constantly stirred for 30 min in the presence of N_2 gas. After charging, the reaction set up was completely evacuated with N_2 gas continuously for 10 to 15 times and the reaction was maintained at room temperature for 72h. The solvent was evaporated at the end of the reaction. The solid polymer obtained after the evaporation was re-dissolved with a small amount of THF which was then reprecipitated with methanol. Finally, the precipitated polymer was purified using Soxhlet extraction with methanol overnight. The purified chalcone based $APAEC_8$, $APAEC_{12}$, $APAEF_8$, $TPAEC_8$, $TPAEC_{12}$ and $TPAEF_8$ (PAE CPs) were collected and preserved for further analysis.[22,23]

For the synthesis of chalcone based $APAEC_8$, $APAEC_{12}$, $APAEF_8$, $TPAEC_8$, $TPAEC_{12}$ and $TPAEF_8$ (PAE CPs), the above polymerization procedure was used with the respective monomers and the details are given below. The stoichiometric ratio for the synthesis of the CPs depends on the corresponding molecular weight of the monomers and batch size.

Polymer 1 ($APAEC_8$)

The above polymerization procedure was followed. 1-(4-((2,5-diethynylphenyl)ethynyl)phenyl) ethanone (referred to as compound A1) (50 mg, 0.186 mmol), 1,4-diiodo-2,5-bis(octyloxy)benzene (referred to as compound A2) (109 mg, 0.186 mmol), $Pd(PPh_3)_4$ (6.4 mg, 5.59×10^{-6} mmol) and Cu(I)I (2.2 mg, 1.12×10^{-5} mmol) were used to obtain and purify polymer $APAEC_8$. Yield 88.5 mg (79%). FTIR (KBr, cm^{-1}): 3064, 1604, 1497, 1457 (aromatic); 2927, 2860 and 1412 (C–H stretching of octyl side chains); 1693 (unsaturated ketone); 2202 (C–C triple bond); 1210 (ether bond). GPC: $\bar{M}_w$ = 15 300, $\bar{M}_n$ = 6667 and polydispersity index (PDI) 2.3.

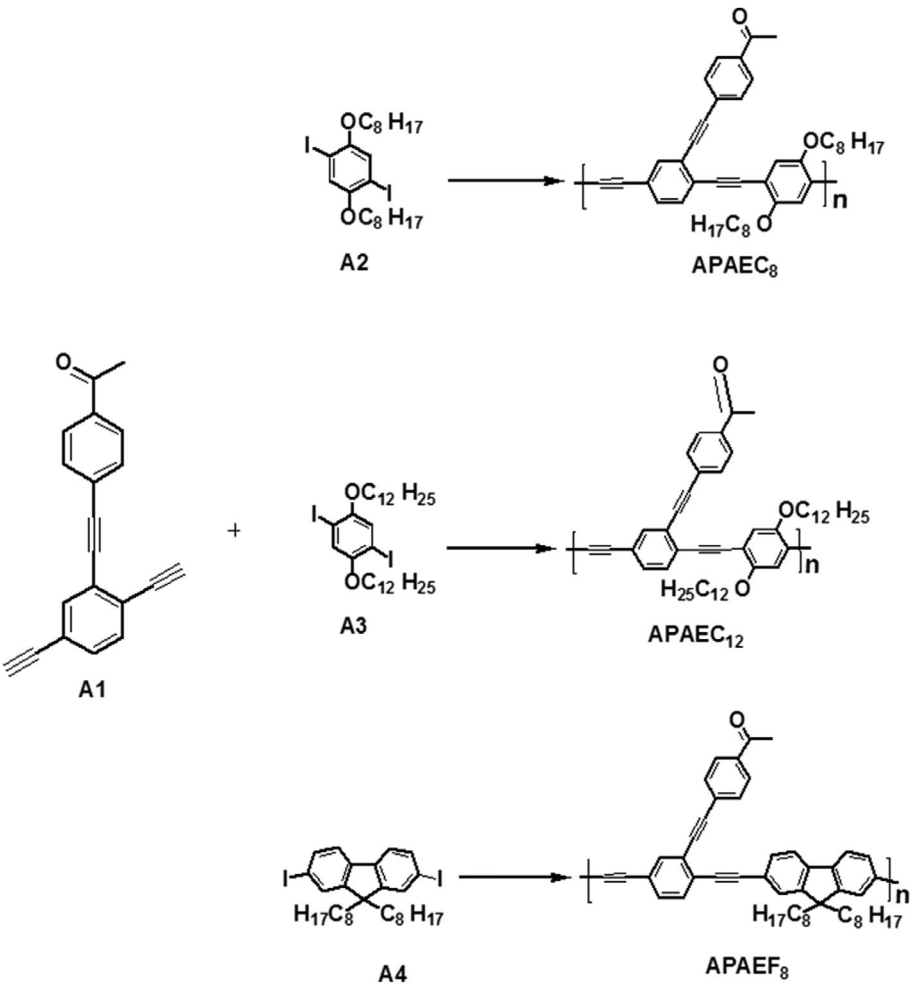

Scheme 1. Synthesis route for $APAEC_8$, $APAEC_{12}$ and $APAEF_8$ (PAE CPs).

Polymer 2 ($APAEC_{12}$)

Compound A1 (50 mg, 0.186 mmol), 1,4-bis(dodecyloxy)-2,5-diiodobenzene (referred to as compound A3) (130 mg, 0.186 mmol), $Pd(PPh_3)_4$ (6.4 mg, 5.59×10^{-6} mmol) and Cu(I)I (2.2 mg, 1.12×10^{-5} mmol) were used to obtain and purify polymer $APAEC_{12}$. Yield 95.0 mg (72%). FTIR (KBr, cm^{-1}): 3042, 1600, 1509, 1464 (aromatic); 2931, 2850, 1105 (C–H stretching of dodecyl side chains); 1696 (unsaturated ketone); 2202 (C–C triple bond); 1214 (ether bond). GPC: $\bar{M}_w = 13\,200$, $\bar{M}_n = 4728$ and PDI = 2.8.

Polymer 3 ($APAEF_8$)

Compound A1 (50 mg, 0.186 mmol), 2,7-diiodo-9,9-dioctyl-9H-fluorene (referred to as compound A4) (120 mg, 0.186 mmol), $Pd(PPh_3)_4$ (6.4 mg, 5.59×10^{-6} mmol) and Cu(I)I (2.2 mg, 1.12×10^{-5} mmol) were used to obtain and purify polymer $APAEF_8$. Yield 84.22 mg (75.2%). FTIR (KBr, cm^{-1}): 3057, 1604, 1487, 1406 (aromatic); 2925, 2843, 1099 (C–H stretching of octyl side chains); 1696 (unsaturated ketone); 2194 (C–C triple bond). GPC: $\bar{M}_w = 11\,300$, $\bar{M}_n = 3636$ and PDI = 3.1.

Polymer 4 ($TPAEC_8$)

1-(4-((2,5-diethynylphenyl)ethynyl)phenyl)-3-(thiophen-2-yl) prop-2-en-1-one (referred to as compound T1) (50 mg, 0.137 mmol), compound A2 (80 mg, 0.137 mmol), $Pd(PPh_3)_4$ (4.7 mg, 4.18×10^{-6} mmol) and Cu(I)I (1.6 mg, 8.2×10^{-6} mmol) were used to obtain and purify polymer $TPAEC_8$. Yield 59.3 mg (62.5%). FTIR (KBr, cm^{-1}): 3075, 1595, 1498 (aromatic); 2925, 2854 (C–H stretching of octyl side chains); 1648 (unsaturated ketone); 2202 (C–C triple bond); 1209 (ether bond). GPC: $\bar{M}_w = 10\,500$, $\bar{M}_n = 4186$ and PDI = 2.5.

Polymer 5 ($TPAEC_{12}$)

Compound T1 (50 mg, 0.137 mmol), compound A3 (95.7 mg, 0.137 mmol), $Pd(PPh_3)_4$ (4.7 mg, 4.18×10^{-6} mmol) and Cu(I)I (1.6 mg, 8.2×10^{-6} mmol) were used to obtain and purify polymer $TPAEC_{12}$. Yield 65.0 mg (58.6%). FTIR (KBr, cm^{-1}): 3072, 1592, 1506, 1463 (aromatic); 2922, 2857 (C–H stretching of dodecyl side chains); 1656 (unsaturated ketone); 2203 (C–C triple bond); 1208 (ether bond). GPC: $\bar{M}_w = 8800$, $\bar{M}_n = 2450$ and PDI = 3.6.

Polymer 6 ($TPAEF_8$)

Compound T1 (50 mg, 0.137 mmol), compound A4 (88 mg, 0.137 mmol), $Pd(PPh_3)_4$ (4.7 mg, 4.18×10^{-6} mmol) and Cu(I)I (1.6 mg, 8.2×10^{-6} mmol) were used to obtain and purify polymer $TPAEF_8$. Yield 63.6 mg (61.8%). FTIR (KBr, cm^{-1}): 3069, 1590, 1464 (aromatic); 2924, 2849 (C–H stretching of octyl side chains); 1660 (unsaturated ketone); 2209 (C–C triple bond). GPC: $\bar{M}_w = 7300$, $\bar{M}_n = 2216$ and PDI = 3.3.

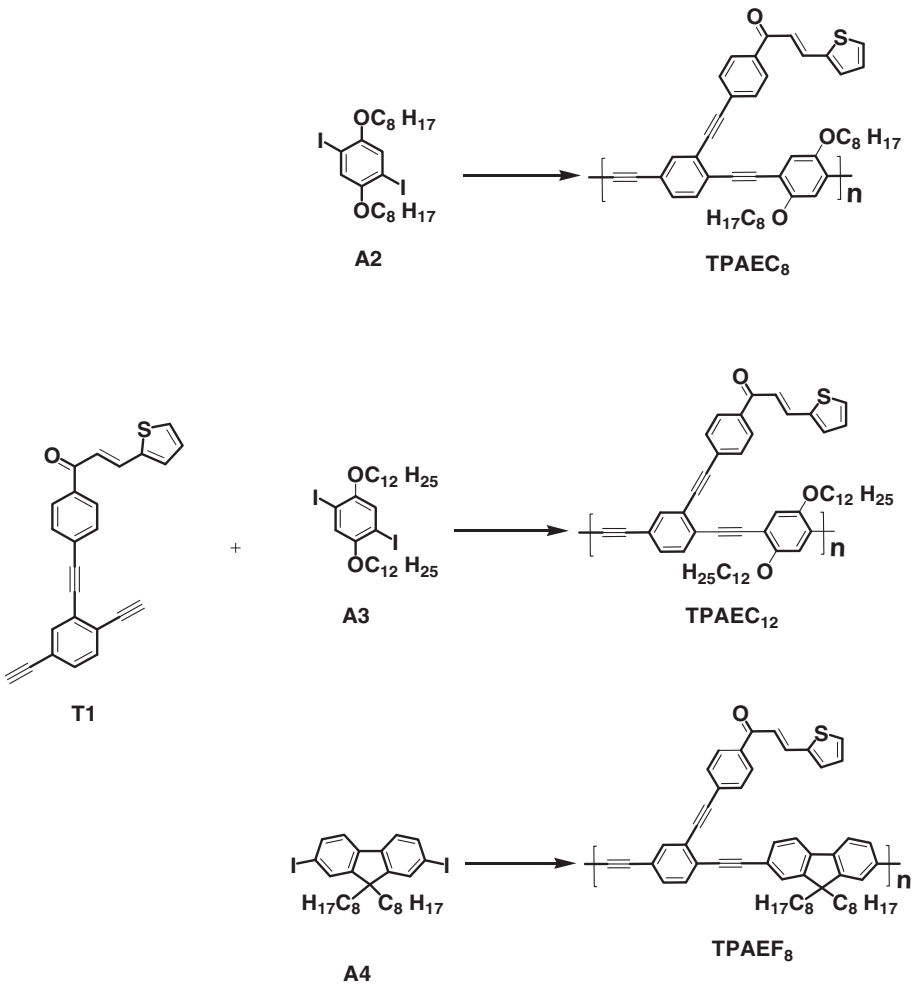

Scheme 2. Synthesis route for $TPAEC_8$, $TPAEC_{12}$ and $TPAEF_8$ (PAE CPs).

RESULTS AND DISCUSSION

Thermogravimetric analysis

The TGA data presented in Fig. 1 indicate that $APAEC_8$, $APAEC_{12}$, $APAEF_8$, $TPAEC_8$, $TPAEC_{12}$ and $TPAEF_8$ start to decompose at 344, 322, 362, 341, 326 and 342 °C respectively. The thermal stability follows the order $APAEF_8$ > $APAEC_8$ > $TPAEF_8$ > $TPAEC_8$ > $TPAEC_{12}$ > $APAEC_{12}$. The thermal stability of the PAE CPs is based on the influence of D–A interactions in the CP chain units and the change of chain conformation upon the reaction of side-chain alkynes. The derivative thermogravimetry curves of $APAEC_8$, $APAEC_{12}$, $APAEF_8$, $TPAEC_8$, $TPAEC_{12}$ and $TPAEF_8$ PAE CPs are shown in Fig. 2.

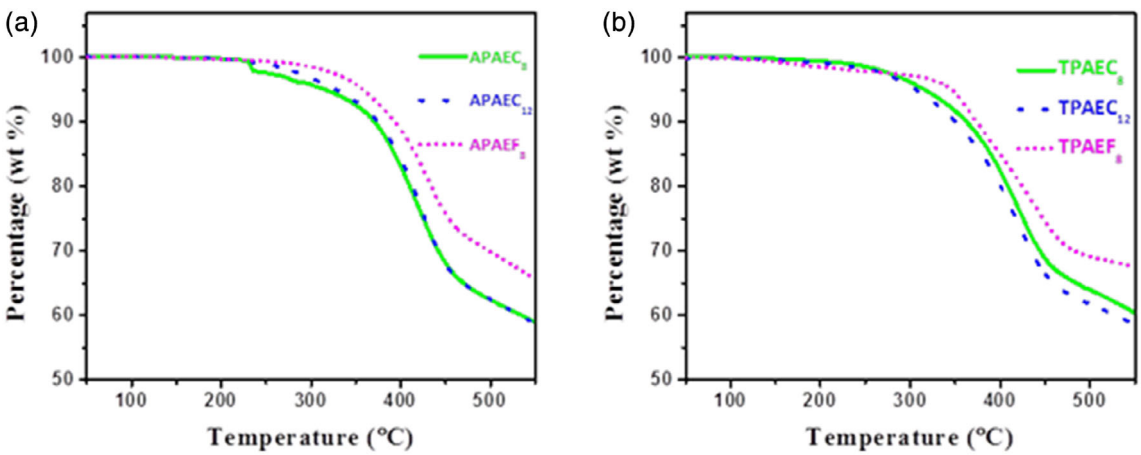

Figure 1. TGA of PAE CPs: (A) $APAEC_8$, $APAEC_{12}$ and $APAEF_8$; (B) $TPAEC_8$, $TPAEC_{12}$ and $TPAEF_8$.

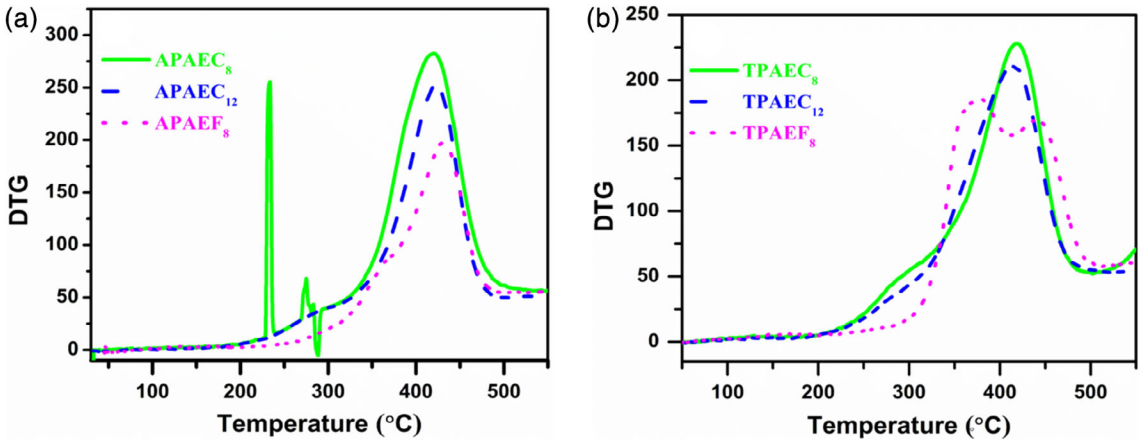

Figure 2. Differential thermogravimetry curve of PAE CPs: (A) $APAEC_8$, $APAEC_{12}$ and $APAEF_8$; (B) $TPAEC_8$, $TPAEC_{12}$ and $TPAEF_8$.

The thermal stability sequence was influenced by the attachment of side-arm substitution, the rigid main backbone chain of the polymers and the greater number of alkoxy chains introduced into the polymer backbone. A high thermal withstanding capacity of conducting polymers was essential for material application. A high thermal stability of conducting polymers is essential for their practical application.[24]

Photophysical properties of CPs

The optical behaviour of the PAE CPs was studied by UV–visible and PL spectra, and the data obtained are presented in Fig. 3. The solid state (thin film) UV–visible spectral measurements were also characterized and are given in Fig. 4. The spectral values of $APAEC_8$, $APAEC_{12}$, $APAEF_8$, $TPAEC_8$, $TPAEC_{12}$ and $TPAEF_8$ (PAE CPs), namely absorption maxima ($\lambda_{abs,max}$), absorption onset ($\lambda_{abs,onset}$) and band gap (E_g) values of the solution and thin films, the fluorescence maxima ($\lambda_{em,max}$) for the solution and the Stokes shift, are presented in Table 1.

Based on observation of the solution phase CP absorption, fluorescence and Stokes shift values, the CPs are arranged in the order $\lambda_{abs,max}$ $APAEC_8$ (425 nm) > $APAEC_{12}$ (421 nm) > $APAEF_8$ (403 nm) > $TPAEF_8$ (361 nm) > $TPAEC_{12}$ (355 nm, 428 nm) > $TPAEC_8$ (354 nm, 427 nm) and in the case of fluorescence are $\lambda_{em,max}$ $APAEF_8$ (470 nm) > $TPAEC_8$ (469 nm), $TPAEC_{12}$ (469 nm) > $APAEC_8$ (467 nm) > $APAEC_{12}$ (466 nm) > $TPAEF_8$ (433 nm, 457 nm). From the data obtained from spectral analysis, it is ascertained that deviations in the π–π^* electronic transition of the CPs were observed due to the side-arm functional groups of acetyl, chalcone thiophene and the main backbone of the D–A chains, which possess low lying energy levels of the lowest unoccupied molecular orbital (LUMO) band of the acceptor unit and in turn influence the π–π^* electronic transition of the CPs in the solution phase. The Stokes shift values obtained between $\lambda_{abs,max}$ and $\lambda_{em,max}$ confirm the electron excitation due to the intramolecular charge transfer of D–A units of the CPs in the solution phase which in turn influence the red shift of the CPs. The Stokes shift values are in the following order: $TPAEC_8$ (117 nm) > $TPAEC_{12}$ (114 nm) > $TPAEF_8$ (80 nm) > $APAEC_8$ (51 nm) > $APAEC_{12}$ (47 nm) > $APAEF_8$ (37 nm). The Stokes shift values of the above mentioned CPs showed a decreasing trend, and this behaviour may be explained by the electronic effects contributed by the D–A CP units. Further, it was noticed that the higher Stokes shift values of $TPAEC_8$, $TPAEC_{12}$ and $TPAEF_8$

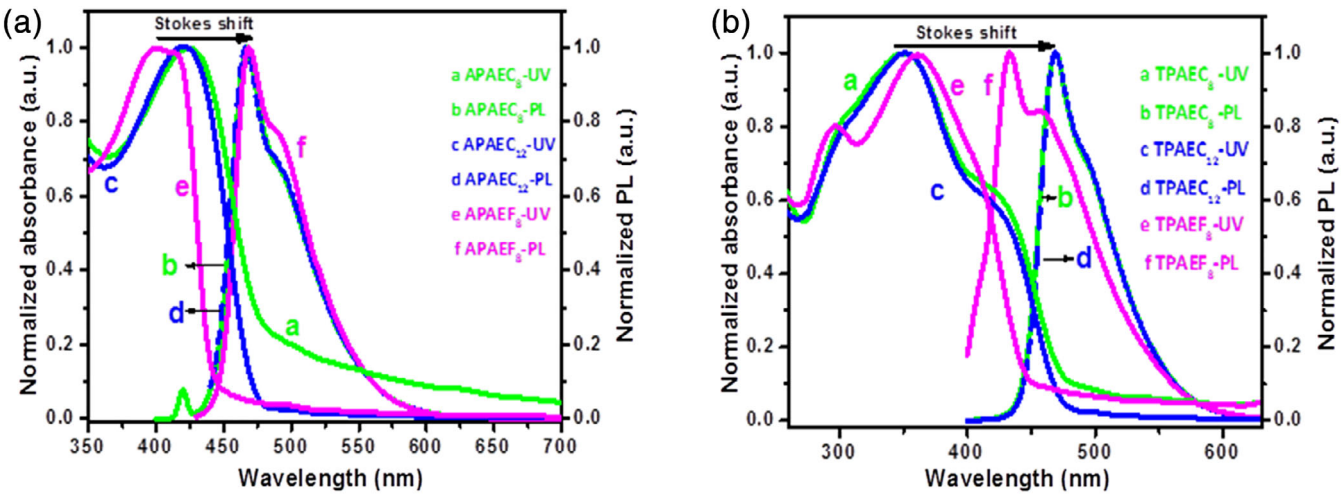

Figure 3. UV–visible (abs) and PL (em) spectra of the CPs in THF solution (0.04 mg in 10 mL): (A) $APAEC_8$, $APAEC_{12}$ and $APAEF_8$; (B) $TPAEC_8$, $TPAEC_{12}$ and $TPAEF_8$.

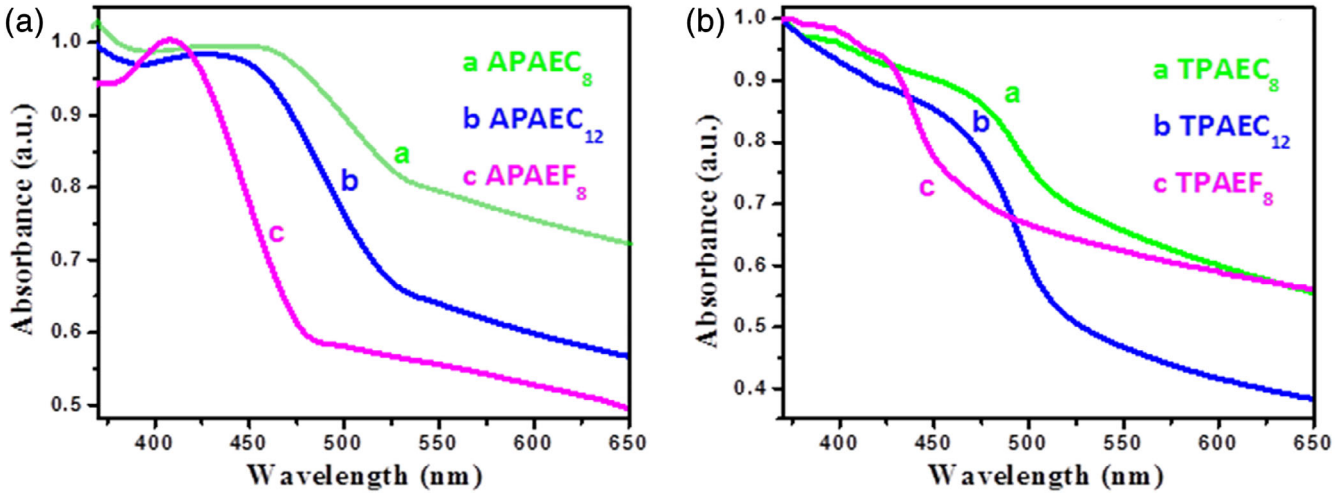

Figure 4. Solid state (thin film) absorption spectra of (A) $APAEC_8$, $APAEC_{12}$ and $APAEF_8$; (B) $TPAEC_8$, $TPAEC_{12}$ and $TPAEF_8$.

were obtained due to the influence of the α, β unsaturated resonance effect.

The data obtained from thin film UV–visible absorption demonstrate a clear understanding of the π–π^* transition of the CPs. The absorption maxima of the thin films were shifted to the red shift region (higher wavelength) from the absorption maxima of the solution phase because of the arrangement of molecules and the conformation behaviour of the CPs. The optical band gap of the CPs was calculated from the UV–visible absorption onset value. The band gap values of the different CPs were arranged in the following order: $TPAEC_8$ (2.112 eV) < $TPAEC_{12}$ (2.322 eV) < $APAEC_8$ (2.339 eV) < $APAEC_{12}$ (2.384 eV) < $TPAEF_8$ (2.421 eV) < $APAEF_8$ (2.605 eV). The lower band gap value of thin film absorption onset was found to be lower than that of the solution phase absorption onset value because of the very tight packing of the thin solid film samples which facilitated a lower band gap than that of the solution phase. $APAEF_8$ and $TPAEF_8$ CPs showed higher band gap values than those of the other CPs because of the presence of the same side attachment of the bisoctyl group of fluorene units which not only induced a self-steric effect but also created conformational changes of the polymer chain.

X-ray diffraction analysis

The structural arrangement of $APAEC_8$, $APAEC_{12}$, $APAEF_8$, $TPAEC_8$, $TPAEC_{12}$ and $TPAEF_8$ (PAE CPs) was interpreted based on the powder XRD analysis. The wide angle and low angle XRD patterns of the CPs are presented in Figs 5 and 6 respectively. The broad peaks obtained from the XRD pattern are $APAEC_8$ (2θ = 8.64°, 22.60° and 42.66°), $APAEC_{12}$ (2θ = 11.18°, 22.06° and 39.06°), $APAEF_8$ (2θ = 8.70°, 22.82° and 42.66°), $TPAEC_8$ (2θ = 21.81°, 30.88°, 42.6° and 49.32°), $TPAEC_{12}$ (2θ = 7.77°, 23.09°, 30.27°, 43.45° and 49.13°) and $TPAEF_8$ (2θ = 10.04°, 22.15°, 30.08°, 41.59° and 48.40°) and these are due to the intermolecular π–π stacking nature of the CPs. The π–π stacking *d*-spacings of the CPs were found to be as follows: $APAEC_8$ 10.22, 3.87 and 2.11 Å; $APAEC_{12}$ 7.9, 4.02 and 2.3 Å; $APAEF_8$ 10.15, 3.89 and 2.11 Å; $TPAEC_8$ 2.89, 2.12 and 1.84 Å; $TPAEC_{12}$ 11.36, 3.84, 2.95, 2.08 and 1.85 Å; and $TPAEF_8$ 8.80, 4.01, 2.96, 2.16 and 1.87 Å. The *d*-value confirmed the coplanar nature of the π–CP chain. The smaller π-stacking value observed may be due to the π–π interaction between the ethynylene bonds of the inter CPs chains. Meanwhile, the presence of alkyl side chains induced the enhanced molecular assembly of the CPs.[25,26]

Scanning electron microscopy (SEM)

The aggregated forms of $APAEC_8$, $APAEC_{12}$, $APAEF_8$, $TPAEC_8$, $TPAEC_{12}$ and $TPAEF_8$ (PAE CPs) were confirmed by SEM. The rough surfaces of the PAE CPs are clearly shown in Fig. 7. The SEM images show the amorphous behaviour of the CPs. The rough surfaces of $APAEC_8$, $APAEC_{12}$, $APAEF_8$, $TPAEC_8$, $TPAEC_{12}$ and $TPAEF_8$ CPs made it difficult to influence the monoclinic lattices, due to structural defects and the amorphous nature of the CPs. The

Table 1. The photophysical properties of PAE CPs

	UV–visible							
CP	λ_{absmax} (solution) (nm)	$\lambda_{absonset}$ (solution) (nm)	E_g (solution) (eV)	λ_{absmax} (film) (nm)	$\lambda_{absonset}$ (film) (nm)	E_g (film) (eV)	λ_{emmax} (solution) (nm)	Stokes shift (nm)
$APAEC_8$	425	476	2.605	460	530	2.339	467	51
$APAEC_{12}$	421	468	2.649	425	520	2.384	466	47
$APAEF_8$	403	440	2.818	408	476	2.605	470	37
$TPAEC_8$	354, 427	471	2.632	365	587	2.112	469	117
$TPAEC_{12}$	355 ,428	469	2.643	371	534	2.322	469	114
$TPAEF_8$	361	441	2.811	373	512	2.421	433,457	80

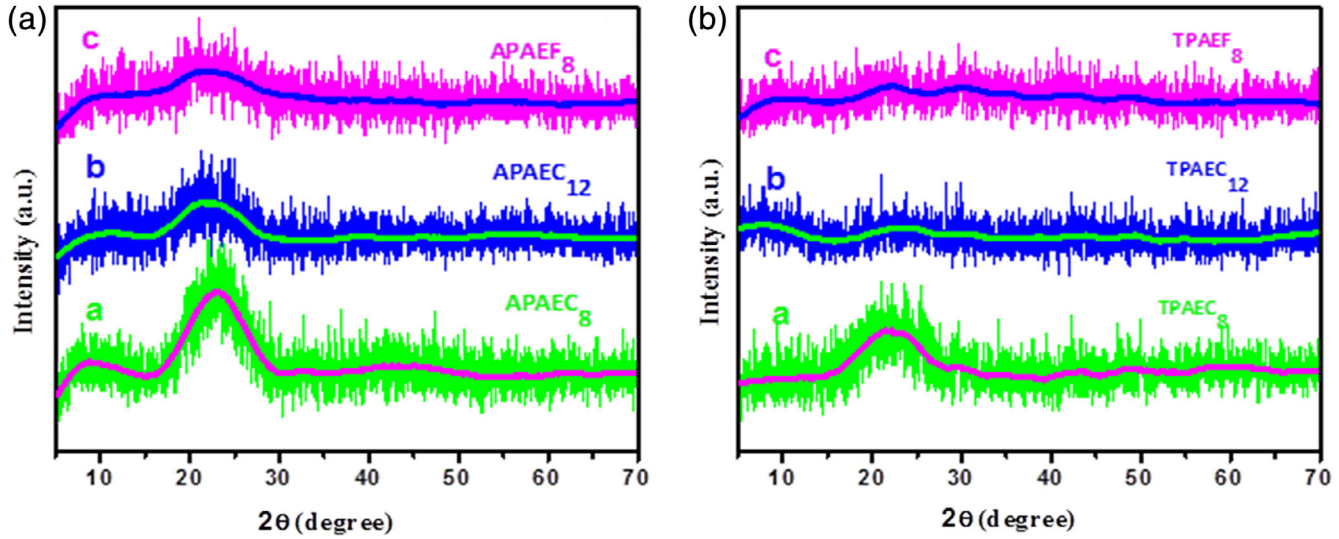

Figure 5. Wide angle powder XRD pattern of (A) $APAEC_8$, $APAEC_{12}$ and $APAEF_8$; (B) $TPAEC_8$, $TPAEC_{12}$ and $TPAEF_8$.

XRD peak and SEM images clearly explain the amorphous nature of the CPs. Based on the morphological results, the incorporation of the side-arm group, conformation changes and chain entanglement of the CPs show the amorphous surface of the CPs which in turn enhances their properties.

Electrochemical properties of the PAE CPs

The redox behaviour of the CPs was studied using cyclic voltammetry measurements. The three-electrode system with tetrabutylammoniumhexylfluorophosphate ($n\text{-}Bu_4NPF_6$) in acetonitrile (100 mmol) was used as an electrolyte and operated at 100 mV s^{-1} of applied potential; this is presented in Fig. 8.

The modified working electrode was prepared by the drop casting method using a CP solution. The thin film assembly and morphological factor depended on the CP chain self-assembly and self-orientation. Further, the presence of alkoxy chains, steric hindrance, average π conjugation and shielding of the CP backbone was explained. These factors influenced the formation of thin films on the working electrode. The chalcone based CPs developed in the present study exhibit irreversible behaviour instead of reversible redox behaviour due to the absence of dication to cation formation. The charge formation on the surface of the modified working electrode is due to the strong anion of the PF_6^- interacting with alkoxy chains and also it depends upon the applied potential and concentration of the electrolyte of the electrochemical system. Further, it was also observed that the charge formation, film assembly, functional group and rigid π system influenced the oxidation onset of the CPs.

Data obtained from the electrochemical studies, namely the oxidation onset, maximum electrochemical peak potential and peak current of the $APAEC_8$, $APAEC_{12}$, $APAEF_8$, $TPAEC_8$, $TPAEC_{12}$ and $TPAEF_8$ CPs, are presented in Table 2. For the para bisoctyloxyphenylene and bisdodecyloxyphenylene unit containing CPs of $APAEC_8$, $APAEC_{12}$, $TPAEC_8$ and $TPAEC_{12}$, the anodic oxidation onset values obtained are 0.791, 0.863, 0.873 and 0.869 V respectively and the maximum anodic peak potential values are 1.107,

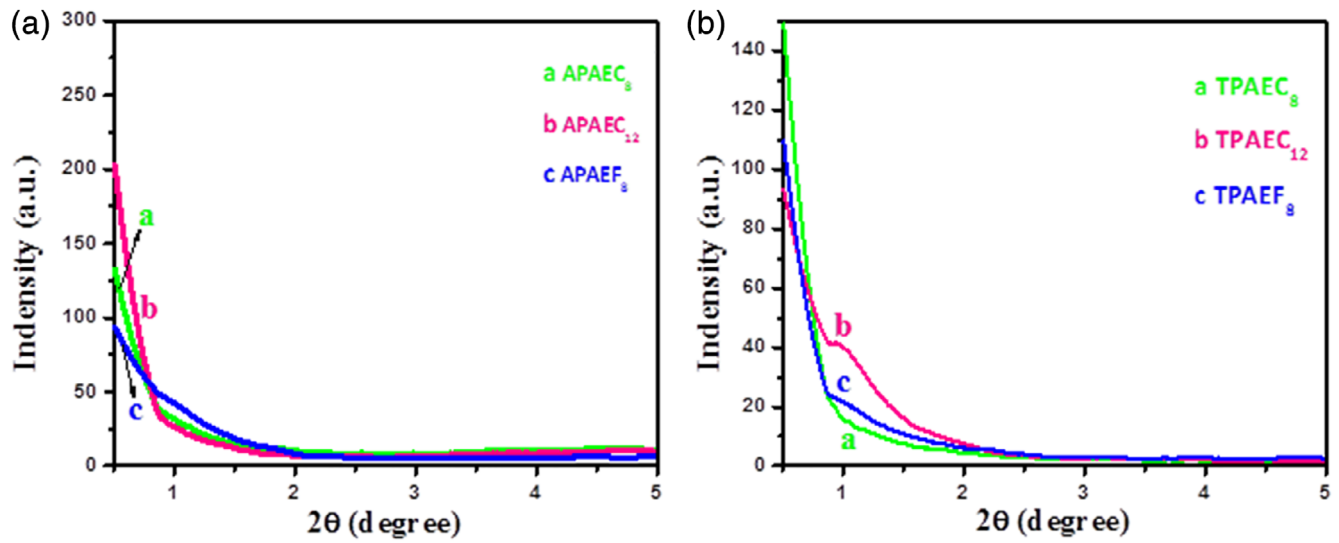

Figure 6. Low angle powder XRD pattern of (A) $APAEC_8$, $APAEC_{12}$ and $APAEF_8$; (B) $TPAEC_8$, $TPAEC_{12}$ and $TPAEF_8$.

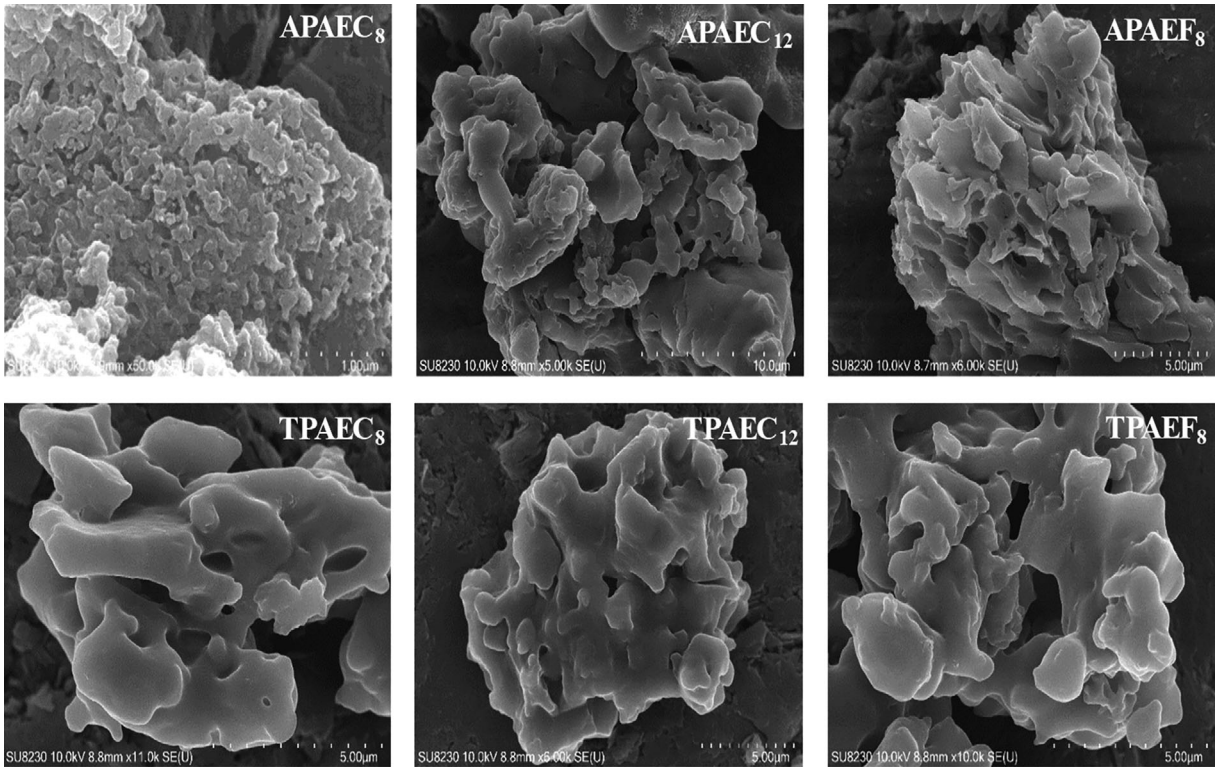

Figure 7. SEM images of $APAEC_8$, $APAEC_{12}$, $APAEF_8$, $TPAEC_8$, $TPAEC_{12}$ and $TPAEF_8$.

1.177, 1.139 and 1.138 V respectively. The maximum anodic peak currents of $APAEC_8$, $APAEC_{12}$, $TPAEC_8$ and $TPAEC_{12}$ are found to be 29.7, 77.9, 61.1 and 94.2 μA, respectively.

The thin film assembly and the side-arm of acetyl and thiophene containing the α, β-unsaturated ketone (chalcone) group contribute to deviations in the electrochemical properties. At the same time, the bisoctylfluorene unit containing CPs $APAEF_8$ and $TPAEF_8$ has different anodic oxidation onset values of 1.153 and1.092 V and maximum anodic peak potential values of 1.309 and 1.405 V with maximum anodic peak current of 80.7 and 51 μA, respectively. The $APAEF_8$ and $TPAEF_8$ CP anodic onset and maximum peak potential values were found to be higher than those of $APAEC_8$, $APAEC_{12}$, $TPAEC_8$ and $TPAEC_{12}$. This may be due to the presence of the same side substituted bisoctyl group and molecular geometry of the CP chain.

The values of the highest occupied molecular orbital (HOMO) and LUMO energy levels of the CPs are presented in Fig. 9. The HOMO value was calculated from the anodic oxidation onset value using Eqn (2) in Appendix S1. The LUMO energy value was determined by substitution of the HOMO energy value and the thin film UV–visible band gap value in Eqn (3) in Appendix S1.

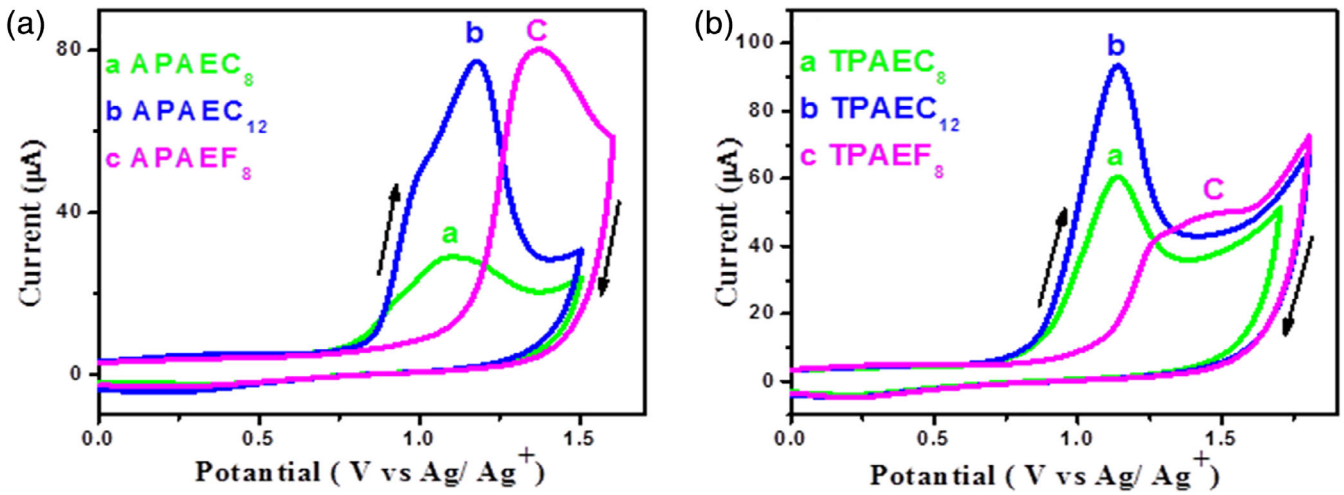

Figure 8. Cyclic voltammograms of the electrochemical oxidation of CPs in 0.1 mol L^{-1} tetrabutylammonium hexafluorophosphate ($TBAPF_6$) in THF with a sweep rate of 100 mV s^{-1}: (A) oxidation properties of $APAEC_8$, $APAEC_{12}$ and $APAEF_8$; (B) oxidation properties of $TPAEC_8$, $TPAEC_{12}$ and $TPAEF_8$.

Table 2. Electrochemical properties from cyclic voltammetry: anodic oxidation (E_{onset}), anodic peak potential (E_{pa}), anodic peak current (I_{pc}), HOMO and LUMO values calculated from Eqns (1) and (2) in Appendix S1

CP	M_n	M_w	PDI M_w/M_n	E_{onset} (V)	E_{pa} (V)	I_{pc} (μA)	HOMO (eV)	LUMO (eV)
$APAEC_8$	6667	15300	2.3	0.791	1.107	29.7	−5.554	−3.204
$APAEC_{12}$	4728	13200	2.8	0.863	1.177	77.9	−5.616	−3.231
$APAEF_8$	3636	11300	3.1	1.153	1.309	80.7	−5.906	−3.300
$TPAEC_8$	4186	10500	2.5	0.873	1.139	61.1	−5.626	−3.513
$TPAEC_{12}$	2450	8800	3.6	0.869	1.138	94.2	−5.622	−3.299
$TPAEF_8$	2216	7300	3.3	1.092	1.405	51	−5.845	−3.423

From this study, the energy levels obtained are arranged in the ascending order $TPAEC_8 < TPAEC_{12} < APAEC_8 < APAEC_{12} < TPAEF_8 < APAEF_8$. The difference in the energy levels of the CPs may be due to the D–A arrangement, π–π stacking entanglement and the presence of the side-arm functional group of CP chains. The bisoctyloxyphenylene unit containing $APAEC_8$ and $TPAEC_8$ has lower HOMO–LUMO energy level compared to the bisdodecyloxyphenylene unit of the $APAEC_{12}$ and $TPAEC_{12}$ CPs due to the presence of a higher chain length of alkoxy groups. If the length of the alkoxy chain exceeds a particular extent, then there might be a possibility of decrease in the free movement of the bisdodecyloxy group which exhibits a higher self-steric effect compared to that of the bisoctyloxy chain. Further, it was also noticed that the CP samples $APAEC_8$ and $TPAEC_8$ have the same alkoxy chain, and the energy level was found to be lower for $TPAEC_8$ compared to $APAEC_8$ due to the presence of thiophene containing α, β unsaturated keto and acetyl groups. A similar trend was also observed for $TPAEC_{12}$ and $APAEC_{12}$. In the cases of $APAEF_8$ and $TPAEF_8$, different substitution takes place compared to the other CPs. The $APAEF_8$ and $TPAEF_8$ CPs exhibited a lower HOMO–LUMO energy level compared to that of the other CPs because of the bisoctyl group substitution on the same side of the fluorene ring. Based on the observations mentioned above, the substitution of alkyl group conformational changes and self-assembly behaviour determines the quality of the thin film formation and charge formation of the working electrode. From this study, it is firmly ascertained that the charge formation on the working electrode occurs at even lower potential for $APAEC_8$, $APAEC_{12}$, $TPAEC_8$ and $TPAEC_{12}$ due to the presence of para-substituted alkoxy chains and reduced steric effect behaviour of the CP chain.

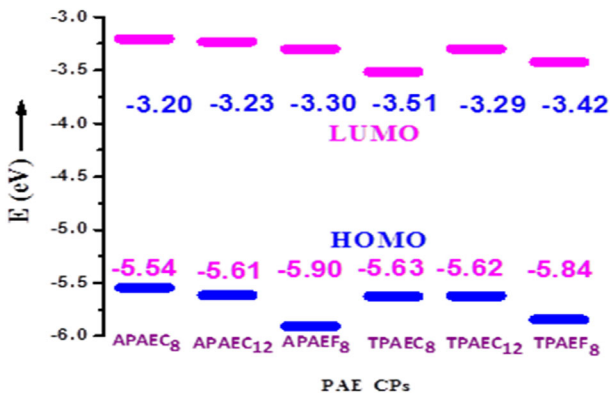

Figure 9. HOMO and LUMO energy level diagram of the PAE CPs $APAEC_8$, $APAEC_{12}$, $APAEF_8$, $TPAEC_8$, $TPAEC_{12}$ and $TPAEF_8$.

CONCLUSION

The six types of $APAEC_8$, $APAEC_{12}$, $APAEF_8$, $TPAEC_8$, $TPAEC_{12}$ and $TPAEF_8$ with rigid two-dimensional PAE CPs were successfully synthesized using palladium catalysed via the Heck–Sonogashira cross-coupling methodology by using diethynylene and diiodo monomers. The molecular structure of the monomers and the average molecular weight of the CPs were determined by standard characterization techniques. The CPs ($APAEC_8$, $APAEC_{12}$, $APAEF_8$, $TPAEC_8$, $TPAEC_{12}$ and $TPAEF_8$) possess unique π–π^* electronic excitation behaviours. Among these CPs $TPAEC_8$ (117 nm) and $TPAEC_{12}$ (114 nm) exhibited higher Stokes shift values than the other CPs. Data obtained from electrochemical and thin film UV–visible spectra were used to determine the optical low band gap and HOMO–LUMO energy levels of the CPs. The CPs $TPAEC_8$ (2.112 eV) and $TPAEC_{12}$ (2.322 eV) possessed better optical band gaps than those of the other CPs. It was also observed that the chalcone based side-arm group of α, β unsaturated keto resonance effect and the uninterrupted electron delocalization of main chain PAE backbone play a vital role in the reduction of the band gap. From the data obtained from different studies, it can be concluded that the PAE CPs $TPAEC_8$ and $TPAEC_{12}$ can be used in photovoltaic and sensor applications.

ACKNOWLEDGEMENT

One of the authors (G. Arun Kumar) thanks the University Grant Commission (UGC) for providing a fellowship under the scheme of UGC-BSR (Proceedings no. 603/PD6/2007).

SUPPORTING INFORMATION

Supporting information may be found in the online version of this article.

REFERENCES

1 Wang C, Dong H, Hu W, Liu Y and Zhu D, *Chem Rev* **112**:2208 (2011).
2 Grimsdale AC, Leok Chan K, Martin RE, Jokisz PG and Holmes AB, *Chem Rev* **109**:897 (2009).
3 Alvey PM, Ono RJ, Bielawski CW and Iverson BL, *Macromolecules* **46**:718 (2013).
4 Hoppe H, Egbe D, Mühlbacher D and Sariciftci N, *J Mater Chem* **14**:3462 (2004).
5 Huber J, Amgoune A and Mecking S, *Adv Mater* **20**:1978 (2008).
6 Huber J and Mecking S, *Angew Chem Int Ed* **45**:6314 (2006).
7 Fiesel R and Scherf U, *Macromol Rapid Commun* **19**:427 (1998).
8 Bunz UH, *Chem Rev* **100**:1605 (2000).
9 Bazzaro M, Anchoori RK, Mudiam MKR, Issaenko O, Kumar S, Karanam B *et al.*, J Med Chem. **54**:449 (2010).
10 Ng H-L, Ma X, Chew E-H and Chui W-K, *J Med Chem* **60**:1734 (2017).

11 Yan J, Chen J, Zhang S, Hu J, Huang L and Li X, J Med Chem. **59**:5264 (2016).
12 Gago S, Pessêgo M r, Laia C s A and Parola AJ, *ACS Omega* **2**:122 (2017).
13 Zhang H, Su J, Lin Y, Bai H, Liu J, Chen H *et al*., *Anal Chem* **89**:6099 (2017).
14 Gan X, Hu D, Wang Y, Yu L and Song B, *J Agric Food Chem* **65**:43 (2017).
15 Basílio N, Gago S, Parola AJ and Pina F, *ACS Omega* **2**:70 (2017).
16 Dini D, Calvete MJF and Hanack M, *Chem Rev* **116**:13043 (2016).
17 Choi DH and Oh SJ, *Eur Polym J* **38**:1559 (2002).
18 Choi K-S, Kim H-W, Kim Y-B and Kim J-D, *Liq Cryst* **31**:639 (2004).
19 Mihara T, Tsutsumi M and Koide N, *Mol Cryst Liq Cryst* **412**:247 (2004).
20 Selvam R and Subramanian K, *J Polym Sci A Polym Chem* **55**:997 (2017).
21 Song F, Wei G, Jiang X, Li F, Zhu C and Cheng Y, *Chem. Commun* **49**: 5772–5774 (2013).
22 Li H, Powell DR, Hayashi RK and West R, *Macromolecules* **31**:52 (1998).
23 Zhou Q and Swager TM, *J Am Chem Soc* **117**:12593 (1995).
24 Huang W and Chen H, *Macromolecules* **46**:2032–2037 (2013).
25 Yasuda T, Imase T, Nakamura Y and Yamamoto T, *Macromolecules* **38**: 4687–4697 (2005).
26 Yamamoto T, Muramatsu Y, Shimizu T and Yamada W, *Macromol Rapid Commun* **19**:263–266 (1998).

